

# SEJONG OPEN CLUSTER SURVEY (SOS) - V. THE ACTIVE STAR FORMING REGION SH 2-255 – 257

BEOMDU LIM<sup>†1</sup>, HWANKYUNG SUNG<sup>2</sup>, HYEONOH HUR<sup>2</sup>, BYEONG-CHEOL LEE<sup>1,3</sup>, MICHAEL S. BESSELL<sup>4</sup>, JINYOUNG S. KIM<sup>5</sup>, KANG HWAN LEE<sup>6</sup>, BYEONG-GON PARK<sup>1,3</sup>, AND GWANGHUI JEONG<sup>1,3</sup>

<sup>1</sup>Korea Astronomy and Space Science Institute, 776 Daedeokdae-ro, Yuseong-gu, Daejeon 305-348, Korea;  
bdlim1210@kasi.re.kr

<sup>2</sup>Department of Astronomy and Space Science, Sejong University, 209 Neungdong-ro, Gwangjin-gu, Seoul 143-747, Korea;  
sungh@sejong.ac.kr

<sup>3</sup>Astronomy and Space Science Major, University of Science and Technology, Gajeong-ro, Yuseong-gu, Daejeon 305-333, Korea

<sup>4</sup>Research School of Astronomy and Astrophysics, Australian National University, MSO, Cotter Road, Weston, ACT 2611, Australia

<sup>5</sup>Steward Observatory, University of Arizona, 933 N. Cherry Ave. Tucson, AZ 85721-0065, USA

<sup>6</sup>Gwacheon National Science Museum, 110 Sanghabeol-ro, Gwacheon-si, Gyeonggi-do 427-060, Korea

Received 2015; accepted 2015

**Abstract:** There is much observational evidence that active star formation is taking place in the HII regions Sh 2-255 – 257. We present a photometric study of this star forming region (SFR) using imaging data obtained in passbands from the optical to the mid-infrared in order to study the star formation process. A total of 218 members were identified using various selection criteria based on their observational properties. The SFR is reddened by at least  $E(B - V) = 0.8$  mag, and the reddening law toward the region is normal ( $R_V = 3.1$ ). From the zero-age main sequence fitting method it is confirmed that the SFR is  $2.1 \pm 0.3$  kpc from the Sun. The median age of the identified members is estimated to be about 1.3 Myr from comparison of the Hertzsprung-Russell diagram (HRD) with stellar evolutionary models. The initial mass function (IMF) is derived from the HRD and the near-infrared ( $J, J - H$ ) color-magnitude diagram. The slope of the IMF is about  $\Gamma = -1.6 \pm 0.1$ , which is slightly steeper than that of the Salpeter/Kroupa IMF. It implies that low-mass star formation is dominant in the SFR. The sum of the masses of all the identified members provides the lower limit of the cluster mass ( $169 M_\odot$ ). We also analyzed the spectral energy distribution (SED) of pre-main sequence stars using the SED fitting tool of Robitaille et al. and confirm that there is a significant discrepancy between stellar mass and age obtained from two different methods based on the SED fitting tool and the HRD.

**Key words:** open clusters and associations: individual: Sh 2-255 – 257 (IC 2162) – dust, extinction – stars: luminosity function, mass function.

## 1. INTRODUCTION

Young open clusters provide useful test beds for the study of star formation processes because about 80 – 90% of young stars are found in embedded clusters with more than 100 members (Lada & Lada 2003; Porras et al. 2003). Furthermore, the fundamental parameters of clusters such as reddening, distance, and age can be properly constrained. These advantages allow us to derive a more reliable stellar initial mass function (IMF) with which to investigate star formation processes.

Sh 2-254 – 258 is a famous star forming region (SFR) in the Gem OB1 association (Sharpless 1959). The main ionizing sources of the HII regions are known to be one late-O and four early-B-type stars (Chavarría et al. 2008). A number of previous works found a few maser

sources (Turner 1971; Lo & Burke 1973; Goddi et al. 2007) as well as various molecular lines (Morris et al. 1974; Blair et al. 1975; Evans et al. 1977; Bieging et al. 2009; Zinchenko et al. 2012) in the region. Several sub-structures such as clumps and cores were also reported from infrared (IR), sub-millimeter, millimeter, and centimeter observations (Beichman et al. 1979; Jaffe et al. 1984; Howard et al. 1997; Minier et al. 2005; Zinchenko et al. 2012). These observational properties commonly indicate that active star formation is in progress.

Chavarría et al. (2008) took a census of young stellar objects (YSOs) using extensive near- to mid-IR imaging data. Most of the young stars ( $\sim 80\%$ ) were found in several embedded sub-clusters. Mucciarelli et al. (2011) continued their search for low-mass YSOs in the quiescent phase, with a deep *Chandra* X-ray observation, and found that the total number of YSOs was consistent with that expected from the Kroupa IMF (Kroupa 2001) scaled to the num-

CORRESPONDING AUTHOR: Beomdu Lim

<sup>†</sup>Korea Research Council of Fundamental Science & Technology Research Fellow

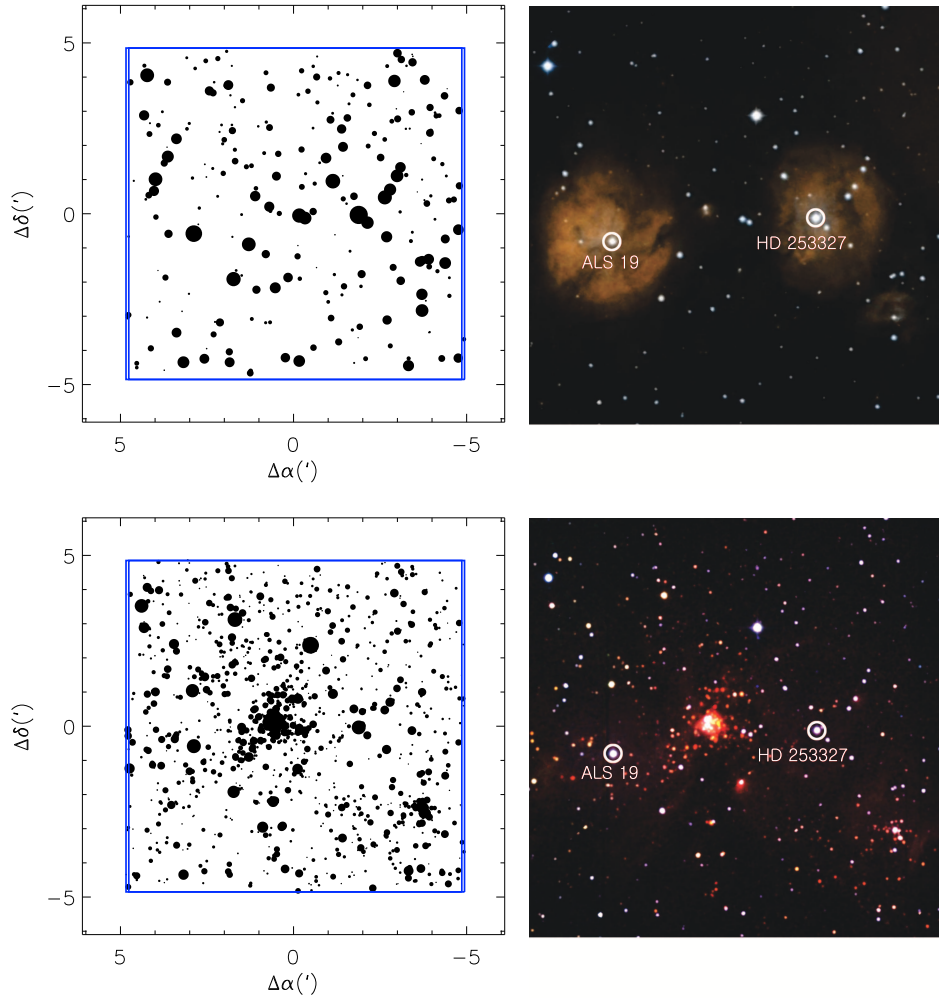


**Figure 1.** Finder chart and color composite image of the observed region in optical passbands (upper) and near-infrared passbands (lower). Stars brighter than  $V = 18$  mag and  $K_S = 16$  mag are plotted in left-hand panels, respectively. The size of the circles is proportional to the brightness of individual stars. The position of stars are relative to  $\alpha = 06^{\text{h}} 12^{\text{m}} 52^{\text{s}}.1$ ,  $\delta = +17^{\circ} 59' 16''.4$ . Squares outlined by blue solid lines represent the field of view of the Mont4K CCD camera. The color composite images were obtained from the Digital Sky Survey-2 and Two Micron All Sky Survey. The position of two ionizing sources is marked by open circles in each image.

ber of ionizing sources. On the other hand, sequential star formation scenarios within the SFR have been proposed (Howard et al. 1997; Minier et al. 2007; Chavarría et al. 2008; Bieging et al. 2009; Wang et al. 2011; Mucciarelli et al. 2011). Circumstantial evidence, such as the age difference among HII regions, and the number ratio of YSOs at different evolutionary stages, indicate that star formation activity propagated from Sh 2-255 and 257 into the molecular clouds behind the HII bubbles. Hence, this SFR is one of the more interesting sites in which to study star and cluster formation processes.

The present work on the embedded young open clusters in the HII regions Sh 2-255 – 257 (hereinafter IC 2162) is the sixth paper of the Sejong Open cluster Survey (SOS) project. Sung et al. (2013a, hereinafter Paper 0) presented the overview of the SOS project.

Comprehensive studies of several open clusters IC 1848, NGC 1624, NGC 1893, NGC 1931, and NGC 2353 were carried out as part of the project (Lim et al. 2011, 2014a,b, 2015). In this current work, we revise the fundamental parameters of the SFR in a homogeneous manner, and constrain the IMF to study star formation processes. The observational data we used are described in Section 2. In Section 3, we present several fundamental parameters of IC 2162 obtained from photometric diagrams and discuss the reddening law toward the SFR. The IMF is derived in Section 4, and the spectral energy distribution (SED) of pre-main sequence (PMS) members is investigated in Section 5. Finally, the comprehensive results from this study are summarized in Section 6.

**Table 1**  
Atmospheric Extinction Coefficients and Photometric Zero points

Filter	$k_1$	$k_2$	$\zeta$ (mag)
<i>I</i>	$0.045 \pm 0.008$	-	$22.170 \pm 0.009$
<i>V</i>	$0.120 \pm 0.008$	-	$23.560 \pm 0.007$
<i>B</i>	$0.232 \pm 0.008$	$0.023 \pm 0.002$	$23.548 \pm 0.006$
<i>U</i>	$0.444 \pm 0.018$	$0.031 \pm 0.005$	$22.069 \pm 0.008$
H $\alpha$	0.085	-	19.565

## 2. OBSERVATIONAL DATA

### 2.1. Optical Imaging Data

The observations of IC 2162 were made on 2013 February 5, using the Kuiper 61" telescope (f/13.5) of Steward Observatory on Mt. Bigelow in Arizona, USA. Images were taken with the Mont4K CCD camera and 5 filters (Bessell *U*, Harris *BV*, Arizona *I*, and H $\alpha$ ) in a  $3 \times 3$  binning mode. The field of view (FOV) is about  $9.7' \times 9.7'$ . The target images comprise 12 frames that were taken in two sets of exposure times for each band (5 and 180 s  $\times$  2 in *I*, 5 and 180 s  $\times$  2 in *V*, 7 and 300 s in *B*, 30 and 600 s in *U*, and 30 and 600 s in H $\alpha$ ). We also observed several equatorial standard stars (Menzies et al. 1991) at air masses of 1.2 – 2 on the same night in order to transform the instrumental magnitudes to the standard magnitude and colors. Additional standard stars with extremely blue and red colors in the Landolt standard star field Rubin 149 (Landolt 1992) were observed to determine the secondary extinction coefficients.

All the pre-processing to remove the instrumental signals were carried out using the IRAF<sup>1</sup>/CCDRED packages. Simple aperture photometry was performed for the standard stars with an aperture size of  $14.''0$  (16.3 pixels). The primary and secondary atmospheric extinction coefficients were determined from the photometric data of the standard stars using a weighted least-square method. We present the coefficients and photometric zero points in Table 1. Point spread function (PSF) photometry of stars in the target images was performed with a small fitting radius of one full width at half-maximum ( $\leq 1.''0$ ) using IRAF/DAOPHOT. Aperture photometry of bright, isolated stars with a photometric error smaller than 0.01 mag in individual target images was obtained to correct for the aperture difference. The instrumental magnitudes of stars in the target images were transformed to the standard magnitude and colors using the transformation relations as described in Appendix of Lim et al. (2015). The finder chart for the stars brighter than  $V = 18$  mag is shown in the upper left-hand panel of Figure 1.

A total of 811 stars were detected from optical photometry. The completeness of our photometry was

assessed from the luminosity function of all observed stars. The luminosity function exhibits a single linear slope in the magnitude range of  $V = 13 - 19$  mag. If we assume that the linear slope is applicable down to the faint stars, the turn-over magnitude gives the completeness limit. As a result, our photometry seems to be about 90% complete down to  $V = 19.3$  mag.

### 2.2. Optical Spectroscopic Data

The optical spectra of two main ionizing sources (ALS 19 and HD 253327) were obtained on 2015 March 10 with the fiber-fed echelle spectrograph BOES (Bohyun-san Observatory Echelle Spectrograph – Kim et al. 2007) attached to the 1.8 m telescope at Bohyunsan Optical Astronomy Observatory in Korea. A single frame for each target was taken with a  $300 \mu\text{m}$  fiber ( $R = 30,000$ ), and the exposure time was 3600 seconds. The  $3 \times 3$  binning mode allowed us to improve the signal-to-noise ratio of the spectra. For the wavelength calibration, spectra of a ThAr lamp were also acquired on the same night.

Pre-processing and extraction of spectra were made with the IRAF/ECHELLE package. A sigma clipping method was used to minimize the influence of cosmic rays on the individual frames in a given order. We normalized the spectra using the best solution found from a cubic spline interpolation and finally smoothed them by a box size of 33. The spectra of ALS 19 and HD 253327 are shown in Figure 2. For comparison, the spectra of standard stars [AE Aur (O9.5V), HD 36960 (B0.5V), HD 42401 (B2V), and  $\eta$  Aur (B3V) – Walborn 1971; Sota et al. 2011] observed with the same instrument on 2014 October 29 are also plotted in the same figure.

### 2.3. Archival Infrared Data

We transformed the CCD coordinates ( $x_{\text{CCD}}, y_{\text{CCD}}$ ) of the optical photometric data into celestial coordinates ( $\Delta\alpha, \Delta\delta$ ) using the Two Micron All Sky Survey catalogue (2MASS; Skrutskie et al. 2006). Optical counterparts of near-IR sources in the 2MASS catalogue were searched for with a matching radius of  $1''$ . A total of 361 optical counterparts were found.

Chavarría et al. (2008) has made an extensive IR imaging survey across the entire molecular complex incubating the HII regions Sh 2-254 – 258. This survey covers an area of  $25' \times 20'$ . Their catalogue includes the near-IR *JHK<sub>S</sub>* and *Spitzer* InfraRed Array Camera (IRAC) 4-band photometry of 26,821 sources. The near-IR photometry in the IR source catalogue is reasonably tied to the 2MASS photometric system within 0.03 mag. Only stars within the FOV of the optical imaging observations were used in our analysis. A total of 3,426 sources were found within our FOV ( $\sim 9.7' \times 9.7'$ ), of which 792 sources have optical counterparts within a matching radius of  $1''$ . We present the finder chart of these stars in the lower left panel of Figure 1.

A post-BCD (basic calibrated and mosaiced) image of the *Spitzer* Multiband Imaging Photometer (MIPS)

<sup>1</sup>Image Reduction and Analysis Facility is developed and distributed by the National Optical Astronomy Observatories, which is operated by the Association of Universities for Research in Astronomy under cooperative agreement with the National Science Foundation.

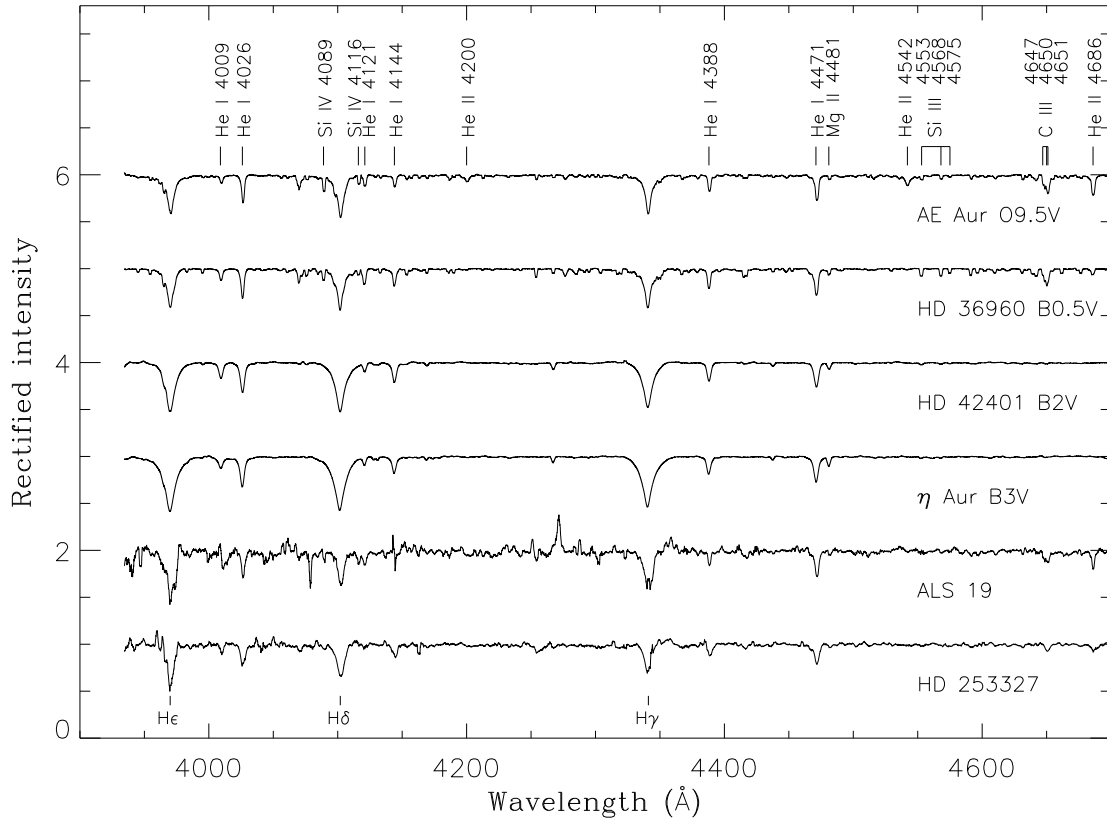


**Figure 2.** Optical spectra of four standard stars and two ionizing sources (from top to bottom) in the observed field of view. The object name is denoted below each spectrum. Main spectral lines used in spectral classification are identified at the top of the figure.

24  $\mu\text{m}$  image was taken from the data archive of the *Spitzer* Science Center (ObsID: 40005, PI G. Fazio). We carried out PSF photometry for stars in the image using the IRAF/DAOPHOT with a fit radius of 2.4 pixel and a sky annulus of  $20'' - 32''$  (see Sung et al. 2009). The photometric zero point of 11.76 mag was calculated using the pixel scale and the flux of a zeroth magnitude star as described in MIPS Handbook. Within our FOV, a total of 207 sources were detected, of which 13 and 30 sources have counterparts in the optical and IR catalogues, respectively.

### 3. FUNDAMENTAL PARAMETERS

As seen in Figure 1, the finder charts and color composite images in the optical and near-IR passbands exhibit completely different stellar distributions. This implies that the majority of young stars are embedded behind the HII regions. Because only about a quarter of the stars were detected in the optical passbands, the canonical analysis based on the optical photometric diagrams is limited. For this reason, the IR photometry of Chavarría et al. (2008), which is less sensitive to the effect of extinction, is a powerful tool to probe embedded populations. However, the several visible stars are still very helpful to determine fundamental parameters

such as reddening and distance. In this section, we describe the identification of the main ionizing sources, membership selection criteria, and the determination of reddening, distance, and age based on the optical spectra and photometric diagrams as presented in Figure 2 – 4.

#### 3.1. Spectral Types of Two Ionizing Sources

The influence of high-mass stars on the surrounding environment involves destructive and constructive processes. The strong stellar wind and radiation pressure of high-mass stars can disperse their natal clouds, and thereby terminate star formation. On the other hand, HII bubbles created by these stars can accumulate and compress material as they expand into the molecular clouds. The condensed material can then form a new generation of stars (Elmegreen & Lada 1977). The high-mass stars can also drive the formation of the second generation of stars radiatively in pre-existing clumps (Lefloch & Lazareff 1994). Therefore, the identification of the ionizing sources is essential for studying such feedback of high-mass stars.

The brightest stars ALS 19 and HD 253327 (ALS 18) are known to be the main ionizing sources of IC 2162. In order to classify the spectral type of these stars, we

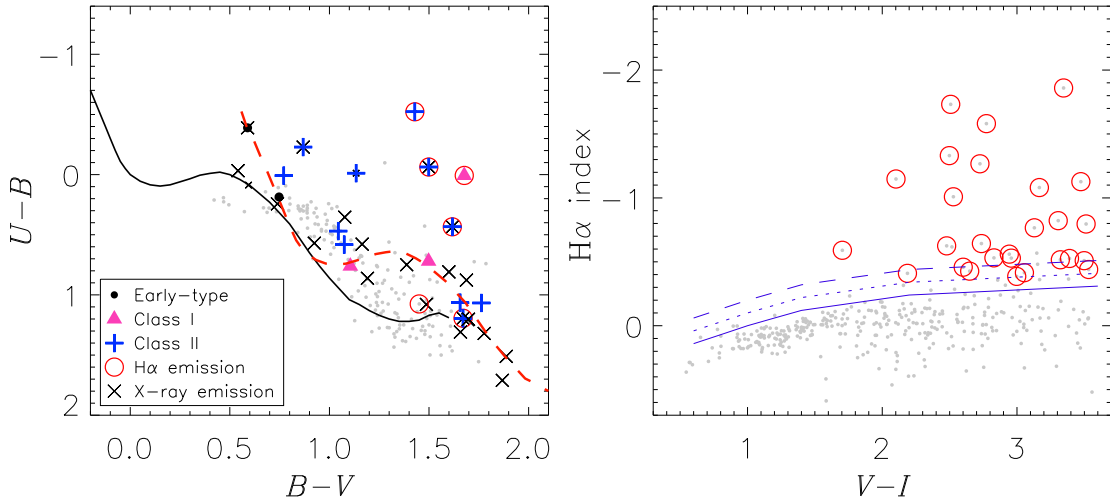


**Figure 3.** Color-color diagrams of stars in IC 2162. The small dots (grey) represent all the stars. Other symbols denote early-type members (black bold dots), Class I (magenta triangles), Class II (blue pluses), X-ray emission stars (large crosses), X-ray emission candidates (small crosses), and  $H\alpha$  emission stars or candidates (red open circles), respectively. The solid line (black) in the left-hand panel exhibits the intrinsic color-color relation of Sung et al. (2013a), and its reddened relation [ $E(B - V) = 0.88$  mag] is shown by a dashed line (red). The solid line in the right-hand panel represents the empirical photospheric level of unreddened main sequence stars, while the dashed and dotted lines are the lower limit of  $H\alpha$  emission stars and  $H\alpha$  emission candidates, respectively.

adopted the O and B-type star classification scheme of Walborn & Fitzpatrick (1990); Sota et al. (2011). The spectra of the stars in Figure 2 contain several emission-like features that are the residuals of cosmic rays. In the case of ALS 19, He II  $\lambda 4200$  and  $\lambda 4542$  are invisible in the spectrum, while He II  $\lambda 4686$  absorption is clearly seen. The spectral type of this star is likely to be B0V; however, it is also possible that ALS 19 is a late-O-type star (O9.5V or O9.7V) given the strength of He II  $\lambda 4686$  and the line ratio between Si IV  $\lambda 4116$  and He I  $\lambda 4121$ . Since the star was classified as Class II (Chavarría et al. 2008), the spectrum of this young star shows a mixture of late-O and early-B-type star characteristics.

He II  $\lambda 4200$  and  $\lambda 4542$  are also absent in the spectrum of HD 253327. Si III  $\lambda 4552$  is invisible, while a weak He II  $\lambda 4686$  absorption is authentically seen. Hence, the spectral type of HD 253327 is likely to be B0V. The spectrum of this star is, indeed, similar to that of ALS 19. Our spectral classification is in a good agreement with that of previous studies (Georgelin et al. 1973; Chavarría et al. 2008).

### 3.2. Membership Selection

Early-type main sequence (MS) stars (putatively B-type stars) can be selected from the optical photometric diagrams (Figure 3 and 4) as they are bright in V and very blue in  $U - B$ . In addition, the reddening and distance of the individual stars can be reliably determined because the intrinsic colors and absolute magnitude of such stars have been well calibrated in the optical passbands. Probable early-type members are firstly selected from magnitude and color cuts as  $V \leq 15$  mag,  $0.5 \leq B - V \leq 0.9$ ,  $-0.6 \leq U - B \leq 0.5$ , and  $Q' \leq -0.3$ ,

where  $Q' \equiv (U - B) - 0.72(B - V) - 0.025E(B - V)^2$  (Paper 0). We then removed several foreground late-type stars (probably F- or G-type) restricting the reddening range to  $E(B - V) > 0.8$  mag and color excess ratios. In addition, a few stars identified as YSOs by Chavarría et al. (2008) were also excluded from the MS member list. Only two stars were finally selected as the early-type MS members of IC 2162.

We utilized  $H\alpha$  photometry as a criterion to identify PMS stars in the SFR. A series of studies demonstrated that  $H\alpha$  photometry can effectively detect a number of low-mass PMS stars at the T Tauri stage in young open clusters (Sung et al. 1997; Sung et al. 1998, 2000; Park et al. 2000; Park & Sung 2002; Sung et al. 2004; Sung & Bessell 2004; Sung et al. 2008; Sung et al. 2013b; Lim et al. 2014a,b, 2015). In order to detect objects with an  $H\alpha$  emission line, the  $H\alpha$  index [ $\equiv H\alpha - (V + I)/2$ ] is used as the detection criterion (Sung et al. 2000). As shown in the right-hand panels of Figure 3, stars with an  $H\alpha$  index smaller than the empirical photospheric level (solid line) of normal MS stars by  $-0.2$  (dashed line), or  $-0.1$  mag (dotted line), was selected as  $H\alpha$  emission stars and candidates, respectively. We found 21  $H\alpha$  emission stars and six candidates. However, the  $H\alpha$  emission star ID 659 ( $V = 18.84$ ,  $V - I = 1.70$ ,  $B - V = 1.45$ , and  $U - B = 1.07$ ) is likely an active late-type star in the field because its colors are similar to those of other field stars. A total of 26  $H\alpha$  emission stars and candidates were selected as PMS members of IC 2162.

Excess emission at IR wavelengths, particularly the mid-IR, is a useful membership selection criterion because a large fraction of PMS stars in young open clus-

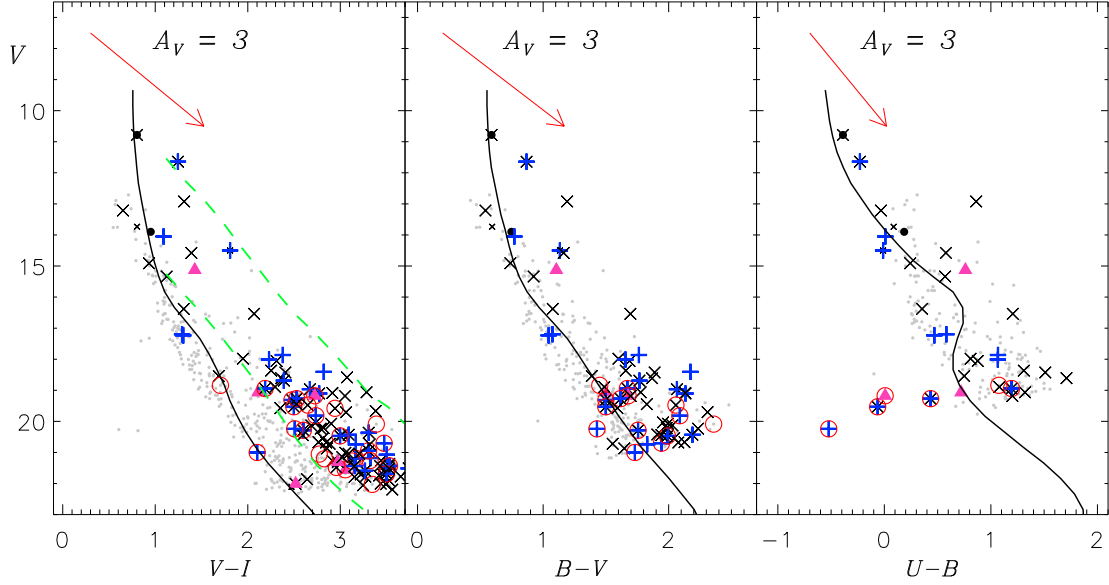


**Figure 4.** Color-magnitude diagrams in the optical passbands. Left-hand panels:  $V - I$  versus  $V$  diagram. The location of pre-main sequence stars is confined between the green dashed lines. Middle panels:  $B - V$  versus  $V$  diagram. Right-hand panels:  $U - B$  versus  $V$  diagram. The solid lines represent the reddened zero-age main sequence relation of Sung et al. (2013a). The arrow denotes the reddening vector corresponding to  $A_V = 3$  mag. The other symbols are the same as Figure 3.

ters ( $\leq 3$  Myr) have been found to have warm circumstellar disks or envelopes (Lada et al. 2000; Sung et al. 2009; Bell et al. 2013). Chavarría et al. (2008) identified 252 YSOs (87 Class I and 165 Class II) in the HII regions Sh 2-254 – 258 using *Spitzer*/IRAC images. We used their YSO list and found optical counterparts for 64 YSOs (11 Class I and 53 Class II) within our FOV. However, only 41 IR sources (6 Class I and 35 Class II) were detected in the  $V$  band.

PMS stars are also known as X-ray emitting objects (Flaccomio et al. 1999; Sung et al. 2004; Caramazza et al. 2012; Hur et al. 2012; Sung et al. 2013b; Lim et al. 2014b; Hur et al. 2015). Mucciarelli et al. (2011) made deep X-ray observations of these SFRs down to  $0.5 M_\odot$  with the *Chandra* X-ray observatory. The observations covered a  $17' \times 17'$  field, and detected a total of 364 X-ray sources. We used their X-ray source list to select X-ray emitting PMS members. The optical counterparts of the X-ray sources and candidates were searched for with matching radii of  $1.''0$  and  $1.''5$ , respectively. We confirmed that 86 X-ray sources and three candidates were detected in the  $V$  band. Among them 73 X-ray sources and one candidate are associated with PMS stars, and the early-type MS star HD 253327 also turns out to be an X-ray source. The other 14 sources and candidates seem to be X-ray active field stars from their colors.

A total of 102 members were identified in the optical passbands. In addition, members of IC 2162 were independently selected from the IR source catalogue of

Chavarría et al. (2008) in the same way. We found 216 members observed in the  $J$  and  $H$  bands (2 early-type MS stars, 20 Class I, 61 Class II, 158 X-ray sources, 7 X-ray candidates, 19  $H\alpha$  emission stars, and 6  $H\alpha$  candidates). The membership list from the IR source catalogue (216 stars) was compared with that from the optical data (102 stars). As a result, 100 stars were found in both lists, however the other two members were observed only in either the  $J$  or  $H$  band. These membership lists were merged into a membership catalogue. The total number of members identified in this work is 218.

Mucciarelli et al. (2011) estimated about 58 field interlopers scaling the number of contaminants in the FOV of the *Chandra* Carina Complex Project (Broos et al. 2011) to that in the FOV of  $17' \times 17'$ . If we assume that the surface density of the field interlopers is uniform across these SFRs, the number of the field interlopers in the FOV of  $\sim 9.7' \times 9.7'$  is about 18. According to the X-ray source classification toward the Carina region (Getman et al. 2011; Broos et al. 2011), extragalactic sources are so faint that the contribution of these sources should be negligible in this study. Probable interlopers in our FOV may therefore be foreground and background stars. However, as the stellar density in the direction of IC 2162 is much lower than that of the Carina region located toward the tangential direction of the Sagittarius spiral arm, the expected number of field interlopers with X-ray emission in our FOV may be much smaller than 18. As we identified 14 X-ray sources and candidates as field interlopers, the

number of field interlopers in our member catalogue may be less than four.

### 3.3. Interstellar Extinction and the Reddening Law

Light from stars is obscured by the interstellar material distributed along the line of sight. Therefore, the effect of extinction on the measured flux or magnitude should be corrected properly. The reddening of young open clusters can be estimated by comparing the observed colors of early-type stars with their intrinsic colors in the  $(U - B, B - V)$  two color diagram along the reddening slope (Paper 0). The reddening determined from two early-type MS members is about  $E(B - V) = 0.88$  mag. In addition, the spectral type of two early-type PMS members ALS 19 (B0V) and 2MASS J06123651+1756548 (B0.9V) is available from this work and Chavarría et al. (2008). The reddening of these stars obtained from the spectral type-color relation (Table 5 in Paper 0) is about  $E(B - V) = 1.41$  and 1.17 mag, respectively. The result is consistent with that of previous studies, e.g.  $E(B - V) = 0.88 - 1.16$  mag (Pismis & Hasse 1976), 0.64 – 1.47 mag (Moffat et al. 1979), and 0.82 – 1.20 mag (Hunter & Massey 1990). More severe differential reddening is expected across IC 2162 because a large number of stars are embedded in the molecular clouds.

The ratio of total-to-selective extinction ( $R_V$ ) is an essential diagnostic tool to investigate the extinction law toward SFRs or young open clusters. The general interstellar medium (ISM) in the solar neighbourhood is known to have, on average,  $R_V = 3.0 - 3.1$  (Fitzpatrick & Massa 2007; Lim et al. 2011). On the other hand,  $R_V$  may be larger than the normal value in some dusty SFRs (Greve 2010). The extinction law depends on the size distribution of dust grains (Draine 2003). A large  $R_V$  implies that the size of dust grains is, on average, larger than that found in the general ISM.

We investigated the various color excess ratios of the early-type MS members to study the reddening law toward IC 2162.  $R_V$  can be determined from the color excess ratios between two different colors (Guetter & Vrba 1989; Sung et al. 2013b). The color excess  $E(V - \lambda)$  (where  $\lambda = I, J, H, K_S, [3.6], [4.5], [5.8],$  and  $[8.0]$ ) can be computed from the intrinsic color relations of Paper 0 and Sung et al. (in preparation). Figure 5 displays the color excess ratios of the early-type MS members.

The color excess ratios at different wavelengths are reasonably matched with the slope corresponding to  $R_V = 3.1$  (solid lines in the figure). This result is acceptable given the  $R_V$  variation with the Galactic longitude (Whittet 1977; Sung & Bessell 2014). The normal reddening law implies that the dust evolution in the front side of the region had already progressed. However, this result may not represent the reddening law of the embedded cluster.

### 3.4. Distance

The distance to an object is fundamental in determining its physical quantities. We determined the distance of IC 2162 using the zero-age main sequence (ZAMS) fitting method. The ZAMS relations and reddening-independent indices introduced in Paper 0 are adopted in the present work. Our ZAMS fitting procedure is based on  $UBVIJHK_S$  multicolor photometry, and therefore the distance can be determined consistently in the optical and near-IR passbands.

Figure 6 shows  $Q_{V\lambda}$ - $Q'$  diagrams of the bright members ( $J < 12.5$ ). Since the luminosity of stars can be affected by stellar evolution and binary effects, the ZAMS relations should be fitted to the lower ridge line of the MS in the  $Q_{V\lambda}$ - $Q'$  planes as shown in the figure. We adjusted the ZAMS relations above and below the faint members at a given  $Q'$  index and adopted a distance modulus of 11.6 mag. The lower ridge line could be confined between the ZAMS relations shifted from the adopted value by  $\pm 0.3$  mag, and therefore the upper and lower envelopes are the uncertainty in the distance. Our result ( $2.1 \pm 0.3$  kpc) is in reasonable agreement with that of previous studies within the uncertainties, e.g. 1.9 kpc (Chavarría-K et al. 1987; Armandroff & Herbst 1981), 2.4 kpc (Hunter & Massey 1990), and 2.5 kpc (Pismis & Hasse 1976; Moffat et al. 1979; Russeil et al. 2007).

### 3.5. Age

The Hertzsprung-Russell diagram (HRD) provides a comprehensive view of the evolutionary status of stellar system. The reddening of the individual members was corrected for using the weighted mean reddening of four early-type MS and PMS members, where the weight is exponentially decreased as the distance between the early-type stars and a given member increases. We converted the reddening-corrected color-magnitude diagrams (CMDs) in the optical passbands to the HRD using several relations (Bessell 1995; Bessell et al. 1998; Paper 0). The effective temperature  $T_{\text{eff}}$  of a star was basically estimated from the color- $T_{\text{eff}}$  relations, and the spectral type- $T_{\text{eff}}$  relation was also used for the three early-type members ALS 19, HD 253327, and 2MASS J06123651+1756548. The weighted mean value of the temperatures was adopted as the  $T_{\text{eff}}$  of four early-type MS and PMS members. Only the  $V - I$  versus  $T_{\text{eff}}$  relation (Bessell 1995; Bessell et al. 1998) was used for the temperature scale of the PMS members to avoid the effect of excess emission due to accretion activities. Bolometric correction values were estimated from the  $T_{\text{eff}}$  of the individual members using Table 5 of Paper 0.

We present the HRD of IC 2162 in Figure 7. The mass of the main ionizing sources in Sh 2-255 and 257 is larger than  $10M_{\odot}$ . It is difficult to estimate the age from the MS turn-off because the stars seem to be still at the MS or PMS stage. On the other hand, the majority of the PMS members are evolving along Hayashi



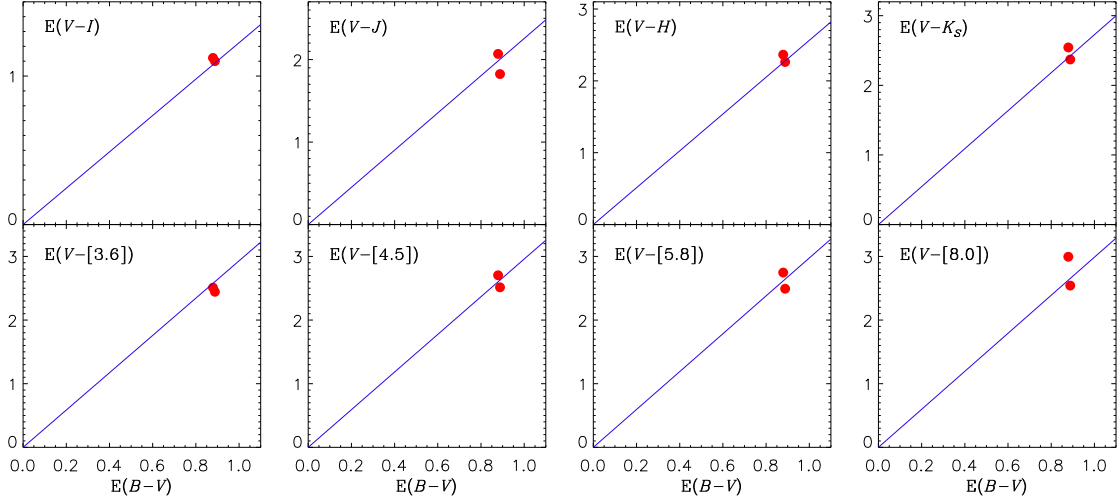


**Figure 5.** Color excess ratios obtained from the early-type main sequence members. The solid line corresponds to  $R_V = 3.1$ . The color excess ratios from optical to mid-infrared data suggest that the reddening law toward IC 2162 is normal.

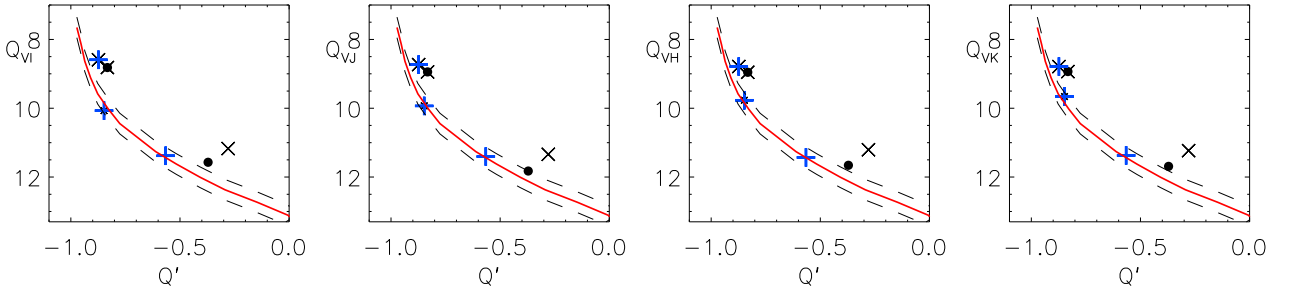


**Figure 6.** Zero-age main sequence (ZAMS) fitting to the bright members in the  $Q_{V\lambda}$ - $Q'$  diagrams. The ZAMS relations of Sung et al. (2013a) are fitted to the lower ridge line of the members. The solid line (red) represents the adopted distance modulus of 11.6 mag, equivalent to 2.1 kpc. The dashed lines indicate a 0.3 mag error in the ZAMS fitting. The other symbols are the same as Figure 3.

tracks, while only several members are approaching the ZAMS along Henyey tracks. There are five PMS members near or below the ZAMS. These stars may have edge-on disks (Sung et al. 1997; Sung & Bessell 2010). The upper mass range of the PMS members appears to be as large as  $15M_{\odot}$ , and the PMS lifetime of high-mass stars is very short. These facts imply that IC 2162 is very young. Using the evolutionary models for PMS stars (Siess et al. 2000,  $Z = Z_{\odot}$  with convective overshooting), we estimated the ages of the PMS members and found a median age of 1.3 Myr with an age spread of 3.3 Myr. The age distribution is very similar to that obtained from the evolutionary models for half solar metallicity ( $Z = 0.01$ ). The age of IC 2162 is probably about 1 Myr. However, as the majority of PMS members are still deeply embedded in the molecular clouds, the age of these stars may be much younger.

#### 4. TOTAL MASS AND THE INITIAL MASS FUNCTION

The masses of optically visible members are estimated by comparing their  $T_{\text{eff}}$  and  $M_{\text{bol}}$  with those of the evolutionary tracks in the HRD. The evolutionary tracks of Ekström et al. (2012) were used for the early-type MS and PMS members, while those of Siess et al. (2000) were adopted for the low-mass PMS members. The solar metallicity was assumed for both models. These theoretical evolutionary masses can be used as a good mass scale reference for those inferred from the near-IR data.

The masses of the members selected from the IR source catalogue were inferred from the  $(J, J - H)$  diagram because the  $J$  magnitude is less affected by excess emission from a disk or envelope compared to the  $K$  magnitude (Kim et al. 2007). Figure 8 shows the near-IR CMD of IC 2162. The PMS members have a wide color range from  $J - H = 0.5$  to 2.9. A few factors such as high differential reddening, excess emission from disks and envelopes in the  $H$  band,



age spread, and photometric errors for faint stars may be responsible for such a large color spread. Only stars brighter than  $J = 16.5$  mag were used so as to minimize the inclusion of stars with large photometric errors. In order to treat differential reddening, a model grid was constructed from several isochrones reddened by  $E(J - H) = 0.25, 0.64, 0.96, 1.27$ , and  $1.91$  mag [equivalently  $E(B - V) = 0.8, 2.0, 3.0, 4.0, 6.0$  mag], respectively.

We attempted to estimate the masses of the PMS members, especially those in the embedded subclusters, using the model grid and compared the masses with those obtained from the optical data. We found the difference between the mass inferred from the near-IR CMD and that from the HRD to be a strong function of the age of the adopted isochrones, due to the luminosity evolution of PMS stars. For a given PMS star, the mass estimated from the reddened isochrone is larger for older isochrones. We found that the difference in masses from the two different methods showed a minimum for a grid of  $0.1$  Myr isochrones.

On the other hand, the mass of PMS stars ( $J > 11.5$  mag) bluer than  $J - H = 1.59$  was obtained from the grid of isochrones with different ages ( $0.1, 0.5, 1, 2, 5$ , and  $10$  Myr) assuming the minimum reddening of  $E(J - H) = 0.25$  mag, equivalent to  $E(B - V) = 0.8$  mag. We compared the masses of all the PMS members with those from the optical data, and confirmed that there was a systematic difference of  $-0.3$  to  $0.4 M_{\odot}$  between them over the mass range of  $0.2$  to  $1.6 M_{\odot}$ . The systematic difference could be approximated by a combination of two straight lines. The mass from the near-IR data was converted to the mass scale obtained from the optical data using those relations. Finally, the masses of four early-type members and two members observed only in either  $J$  or  $H$  were obtained from analysis of the optical data.

In order to examine the metallicity effect on the mass estimation, we also inferred the masses of the PMS stars using the PMS star evolution models for the half solar metallicity. The mass difference from the two models ( $Z = Z_{\odot}$  and  $Z = 1/2 Z_{\odot}$ ) is about  $0.13 M_{\odot}$ . It was confirmed that this difference yields a negligible effect on the resultant IMF in the mass range of  $1 - 100 M_{\odot}$ .

We obtained the cluster mass of  $169 M_{\odot}$  from the sum of the masses of all the identified members. This is definitely a lower limit because a number of sub-solar mass stars below the completeness limit were not considered. IC 2162 seems to be the smallest SFR among the young open clusters studied by our research group, e.g.,  $> 510 M_{\odot}$  for NGC 1624 and NGC 1931 (Lim et al. 2015),  $> 576 M_{\odot}$  for NGC 2264,  $> 1,300 M_{\odot}$  for NGC 1893 (Lim et al. 2014b),  $> 2,600 M_{\odot}$  for NGC 6231 (Sung et al. 2013b),  $> 7,400 M_{\odot}$  for Westerlund 2 (Hur et al. 2015), and  $> 50,000 M_{\odot}$  for Westerlund 1 (Lim et al. 2013).

The IMF is, in general, expressed by the following relation (Salpeter 1955):

$$\xi(\log m) \equiv \frac{N}{\Delta \log m \cdot S} \quad (1)$$

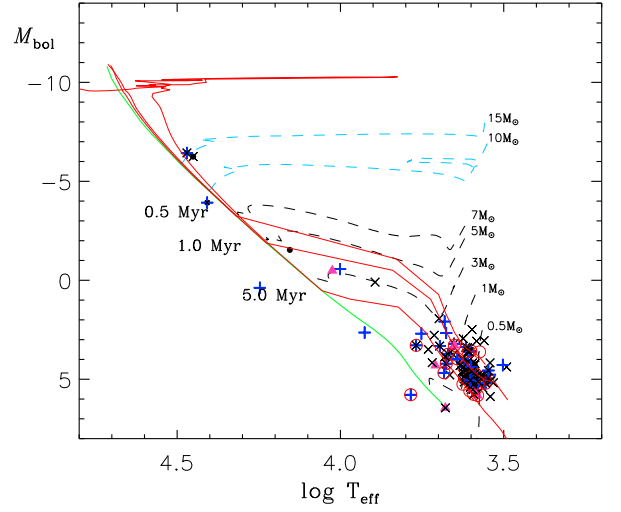


**Figure 7.** Hertzsprung-Russell diagram of IC 2162. A few isochrones (red solid lines) for the age of  $0.5, 1$ , and  $5$  Myr are superimposed on the diagram with the evolutionary tracks of several initial masses (Siess et al. 2000; Ekström et al. 2012), where the solar metallicity is assumed. The other symbols are the same as Figure 3

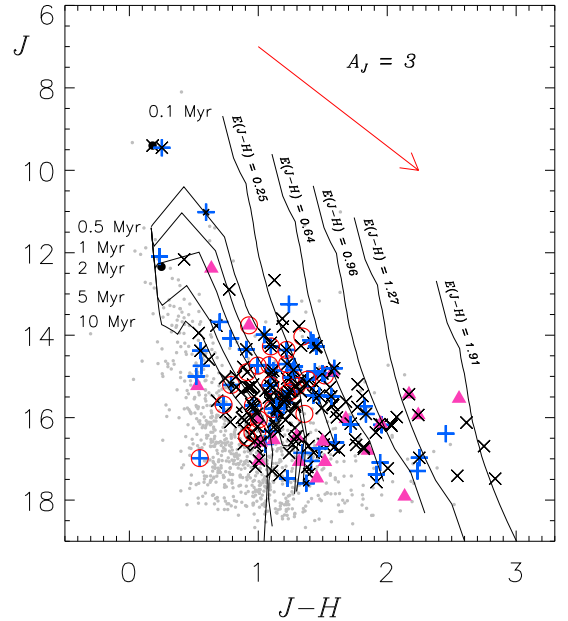


**Figure 8.** Near-infrared color-magnitude diagram. The solid lines represent pre-main sequence star isochrones with different ages ( $0.1, 0.5, 1, 2, 5$ , and  $10$  Myr) from Siess et al. (2000), where the model parameters are the same as seen in Figure 7. The isochrones are reddened by  $E(J - H) = 0.25, 0.64, 0.96, 1.27$ , and  $1.91$  mag, respectively, after correction for the distance modulus of  $11.6$  mag. The arrow denotes the reddening vector corresponding to  $A_J = 3$  mag. The other symbols are the same as Figure 3.

where  $N$ ,  $\Delta \log m$ , and  $S$  represent the number of stars

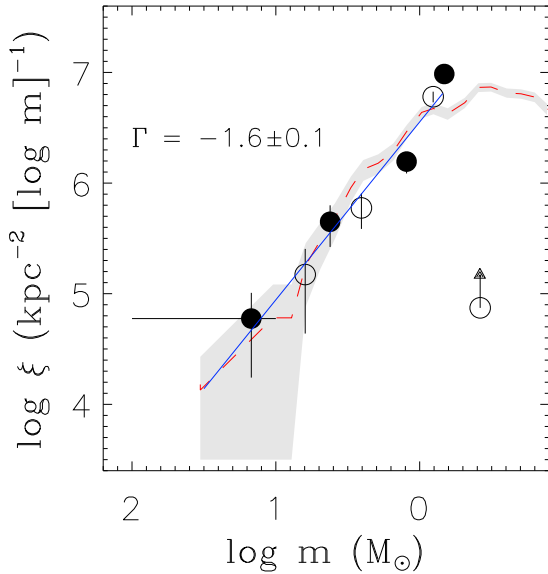


**Figure 9.** The initial mass function (IMF) of IC 2162. The IMF (open and filled circles) was derived using different binning of the same stars to avoid the binning effect. The dashed line and shaded area represent the IMF of NGC 2264 and its uncertainty (Sung & Bessell 2010), respectively. The arrow indicates the IMF below the completeness limit.

in a given mass bin, the size of a logarithmic mass bin, and the area of the observed region, respectively. The size of the mass bin was set to be 0.4 to avoid uncertainties from small sample statistics. We assumed that the upper limit of stellar mass to be  $100M_{\odot}$ , and adopted a larger bin size of 1 for the highest mass bin ( $10 < M/M_{\odot} \leq 100$ ) because the number of high-mass stars was insufficient to sample across various mass bins. We counted the number of stars in each mass bin, and then divided the total by the size of the mass bin and the area of IC 2162 (the area of our FOV). In order to prevent the binning effect, the IMF was re-derived for the same stars by shifting the mass bin by 0.2.

Figure 9 shows the IMF of IC 2162. We also plotted the IMF of the young open cluster NGC 2264 (Sung & Bessell 2010) for comparison. The shapes of the IMFs are similar to each other in the mass range from  $1M_{\odot}$  to the upper limit of stellar mass. The IMF is generally quantified by its slope ( $\Gamma$ ) to compare it with that of other SFRs. We computed the slope of the IMF using a linear least square fitting method. The slope of the IMF is about  $\Gamma = -1.6 \pm 0.1$ . This result is consistent with that of NGC 2264, although the slope is slightly steeper than that of the Salpeter/Kroupa IMF (Salpeter 1955; Kroupa 2001). It implies that the underlying star formation processes in IC 2162 are optimized to produce low-mass stars rather than high-mass stars.

## 5. SPECTRAL ENERGY DISTRIBUTION ANALYSIS

The SED of the members was also analyzed using the SED fitting tool (called the SED fitter) of Robitaille et al. (2007). In order to increase the number of samples, we included 43 stars with X-ray and mid-IR excess emission in the membership catalogue. A total of 261 members were used in this analysis. All the selected members were observed in more than 3 passbands, and their photometric errors were better than 0.15 mag in the optical to near-IR passbands and 0.20 mag in the mid-IR passbands.

In order to minimize the degrees of freedom, we limited the distance to  $2.1 \pm 0.3$  kpc based on the result of the ZAMS fitting above. The total extinction  $A_V$  was set to be  $2.48 - 100$  mag. The SED fitter suggests various models with  $\chi^2$  values for a given SED. To select the most appropriate model among them, we followed the guidelines introduced by Sung & Bessell (2010). The guidelines recommended the model that gives the smallest stellar mass out of the 10 suggested models if  $\chi^2/\chi_{\min}^2 \leq 2.0$ . If  $\chi_{\min}^2$  is less than 1.0, the mass-minimum model with  $\chi^2 < 2.0$  is adopted.

The model adopted from the SED fitter provides various physical quantities of the disks and envelopes as well as stellar parameters (mass and age). The disk parameters such as mass, outer radius, and accretion rate evolve with time by a few orders of magnitude over 10 Myr. A strong correlation between the disk accretion rate and disk mass was also found [ $\log(dM_{\text{disk}}/dt) = -4.89(\pm 0.12) + 1.15(\pm 0.03) \log(M_{\text{disk}}/M_{\star})$ ]. It appears that the envelope mass decreases dramatically after 1 Myr. While the angle of the cavity rises with time, its density, in contrast, declines as a function of time. The circumstellar extinction is proportional to the envelope mass and shows a sharp increase for stars with large envelope mass ( $\log M_{\text{env}}/M_{\star} > -3$ ). Stars with a massive envelope accrete much more material than low-mass counterparts. These correlations between the results obtained from the SED fitter are very similar to those found by Sung & Bessell (2010, see their Figure 3 and 4).

We also compared the stellar mass and age inferred from the SED fitter with those from the analysis of the HRD. For less reddened members, the masses obtained from the different methods are reasonably consistent, while the SED fitter underestimated the ages of the PMS members. On the other hand, the SED fitter tends to overestimate the masses and ages of highly reddened stars. This discrepancy has also been reported by Sung & Bessell (2010, see their Figure 2).

## 6. SUMMARY

IC 2162 is an active SFR in which very young sub-clusters are embedded. We present a multiwavelength study of the SFR as part of the SOS project. This work provided homogeneous optical photometric data as well as a comprehensive result for the young stellar population in IC 2162.

The main ionizing sources in Sh 2-255 and 257 are two B0 stars (ALS 19 and HD 253327). A total of 218 members were identified from the various photometric diagrams, the X-ray source list (Mucciarelli et al. 2011), and the YSO list (Chavarría et al. 2008). It appears from the two early-type MS members that IC 2162 is reddened by at least  $E(B - V) = 0.8$  mag. A large portion of the color spread in the near-IR CMD may be attributed to the presence of severe differential reddening, because a large number of stars are actually embedded in the molecular cloud behind the HII bubbles. The reddening law toward IC 2162 was investigated with various color excess ratios and the ratio of total-to-selective extinction found to be the normal value ( $R_V = 3.1$ ). It implies that the dust evolution in the front side of the SFR has been completed. We also revisited the distance to IC 2162 with the ZAMS fitting method and determined a distance of  $2.1 \pm 0.3$  kpc.

The ages of the members were estimated from the HRD using several evolutionary models (Siess et al. 2000; Ekström et al. 2012) for the solar metallicity. The median age of the optically visible stars in IC 2162 was about 1.3 Myr, and an age spread of 3.3 Myr was found. We derived the IMF of IC 2162 by analyzing the HRD and the  $(J, J - H)$  diagram. The shape of the IMF is similar to that of the nearby young open cluster NGC 2264 in the mass range  $1M_\odot$  to the upper limit of stellar mass. The slope of the IMF was  $\Gamma = -1.6 \pm 0.1$ , which is slightly steeper than that of Salpeter/Kroupa IMF. This result indicates that it was low-mass star formation that mostly took place throughout IC 2162. The lower limit on the cluster mass ( $> 169M_\odot$ ) was also constrained from the sum of the masses of all the identified members.

The SEDs of the members were also analyzed with the SED fitter (Robitaille et al. 2007). The results included the disk and envelope parameters of PMS stars as well as stellar parameters such as age and mass. The properties of the disk and envelope were investigated as a function of stellar age or mass, respectively. The discrepancy between the results from the SED fitter and the analysis based on the HRD was also pointed out.

#### ACKNOWLEDGMENTS

This work was partly supported by a National Research Foundation of Korea grant funded by the Korean Government (Grant No. 20120005318) and partly supported by the Korea Astronomy and Space Science Institute (Grant No. 2015183014).

#### REFERENCES

Armandroff, T. E., & Herbst, W. 1981, Distances to 14 molecular clouds (including two associated with supernova remnants) by a new technique, *AJ*, 86, 1923  
 Beichman, C. A., Becklin, E. E., & Wynn-Williams, C. G. 1979, New multiple systems in molecular clouds, *ApJ*, 232, 47  
 Bell, C. P. M., Naylor, T., Mayne, N. J., Jeffries, R. D., & Littlefair, S. P. 2013, Pre-main-sequence isochrones -

II. Revisiting star and planet formation time-scales, *MNRAS*, 434, 806  
 Bessell, M. S. 1995, The temperature scale for cool dwarfs, in *Proc. ESO Workshop, The Bottom of the Main Sequence and Beyond*, ed. C. G. Tinney (Berlin: Springer), 123  
 Bessell, M. S., Castelli, F., & Plez, B. 1998, Model atmospheres broad-band colors, bolometric corrections and temperature calibrations for O - M stars, *A&A*, 333, 231  
 Bieging, J. H., Peters, W. L., Vilaro, B. V., Schlottman, K., & Kulesa, C. 2009, Sequential star formation in the Sh 254-258 molecular cloud: Heinrich Hertz Telescope maps of CO  $J = 2 - 1$  and  $3 - 2$  emission, *AJ*, 138, 975  
 Blair, G. N., Peters, W. L., & vanden Bout, P. A. 1975, Strong molecular line emission associated with small H $\alpha$  emission regions, *ApJ*, 200, L161  
 Broos, P. B., Getman, K. V., Povich, M. S., Townsley, L. K., Feigelson, E. D., & Garmire, G. P. 2011, A naive Bayes source classifier for X-ray sources, *ApJS*, 194, 4  
 Caramazza, M., Micela, G., Prisinzano, L., Sciortino, S., Damiani, F., Favata, F., Stauffer, J. R., Vallenari, A., & Wolk, S. J. 2012, Star formation in the outer Galaxy: coronal properties of NGC 1893, *A&A*, 539, 74  
 Chavarría, L. A., Allen, L. E., Hora, J. L., Brunt, C. M., & Fazio, G. G. 2008, *Spitzer* observations of the massive star-forming complex S254-S258: Structure and evolution, *ApJ*, 682, 445  
 Chavarría-K, C., de Lara, E., & Hasse, I. 1987, Eight-colour photometry of stars associated with selected Sharpless H II regions at L exp II of about 190 deg - S 252, S 254, S 255, S 257, and S 261, *A&A*, 171, 216  
 Draine, B. T. 2003, Interstellar dust grains, *ARA&A*, 41, 241  
 Ekström, S., Georgy, C., Eggenberger, P., et al. 2012, Grids of stellar models with rotation. I. Models from 0.8 to 120  $M_\odot$  at solar metallicity ( $Z = 0.014$ ), *A&A*, 537, 146  
 Elmegreen B. G., & Lada C. J. 1977, Sequential formation of subgroups in OB associations, *ApJ*, 214, 725  
 Evans, N. J., II, Beckwith, S., & Blair, G. N. 1977, The energetics of molecular clouds. I - Methods of analysis and application to the S255 molecular cloud, *ApJ*, 217, 448  
 Fitzpatrick, E. L., & Massa, D. 2007, An analysis of the shapes of interstellar extinction curve. V. The IR-through-UV curve morphology, *ApJ*, 663, 320  
 Flaccomio, E., Micela, G., Sciortino, S., Favata, F., Corbally, C., & Tomaney, A. 1999, *BVR* photometry of the star-forming region NGC 2264: the initial mass function and star-forming rate, *A&A*, 345, 521  
 Georgelin, Y. M., Georgelin, Y. P., & Roux, S. 1973, Observations de nouvelles régions HII galactiques et d'étoiles excitatrices, *A&A*, 25, 337  
 Getman, K. V., Broos, P. S., Feigelson, E. D., Townsley, L. K., Povich, M. S., Garmire, G. P., Montmerle, T., Yonekura, Y., & Fukui, Y. 2011, Source contamination in X-ray studies of star-forming regions: Application to the Chandra Carina Complex Project, *ApJS*, 194, 3  
 Goddi, C., Moscadelli, L., Sanna, A., Cesaroni, R., & Minier, V. 2007, Associations of H $_2$ O and CH $_3$ OH masers at milli-arcsec angular resolution in two high-mass YSOs, 461, 1027  
 Greve A. 2010, Extinction  $A_V$ , R towards emission nebulae derived from common upper level Paschen-Balmer hydrogen lines, *A&A*, 518, 62  
 Guetter, H. H., & Vrba, F. J. 1989, Reddening and polari-

- metric studies toward IC 1805, *AJ*, 98, 611
- Howard, E. M., Pipher, J. L., & Forrest, W. J. 1997, S255-2: The formation of a stellar cluster, *ApJ*, 481, 327
- Hunter, D. A., & Massey, P. 1990, Small Galactic H II regions. I - Spectral classifications of massive stars, *AJ*, 99, 846
- Hur, H., Park, B.-G., Sung, H., Bessell, M. S., Lim, B., Chun, M.-Y., & Sohn, S. T. 2015, Reddening, distance, and stellar content of the young open cluster Westerlund 2, *MNRAS*, 446, 3797
- Hur, H., Sung, H., & Bessell, M. S. 2012, Distance and the initial mass function of young open clusters in the  $\eta$  Carina nebula: Tr 14 and Tr 16, *AJ*, 143, 41
- Jaffe, D. T., Davidson, J. A., Dragovan, M., & Hildebrand, R. H. 1984, Far-infrared and submillimeter observations of the multiple cores in S255, W3, and OMC-1 - Evidence for fragmentation?, *ApJ*, 284, 637
- Kim, H., Nakajima, Y., Sung, H., Moon, D.-S., & Koo, B.-C. 2007, A near-infrared study of the highly-obscured active star-forming region W51B, *J. Korean Astron. Soc.*, 40, 17
- Kim, K.-M., Han, I., Valyavin, G. G., et al. 2007, The BOES spectropolarimeter for Zeeman measurements of stellar magnetic fields, *PASP*, 119, 1052
- Kroupa, P. 2001, On the variation of the initial mass function, *MNRAS*, 322, 231
- Lada, C., & Lada, E. 2003, Embedded clusters in molecular clouds, *ARA&A*, 41, 57
- Lada, C. J., Muench, A. A., Haisch K. E., Jr, Lada, E. A., Alves, J. F., Tollestrup, E. V., & Willner, S. P. 2000, Infrared *L*-band observations of the Trapezium Cluster: A census of circumstellar disks and candidate protostars, *AJ*, 120, 3162
- Landolt, A. U. 1992, *UBVRI* photometric standard stars in the magnitude range 11.5-16.0 around the celestial equator, *AJ*, 104, 340
- Lefloch B., & Lazareff B. 1994, Cometary globules. 1: Formation, evolution and morphology, *A&A*, 289, 559
- Lim, B., Chun, M.-Y., Sung, H., Park, B.-G., Lee, J.-J., Shon, S. T., Hur, H., & Bessell, M. S. 2013, The starburst cluster Westerlund 1: The initial mass function and mass segregation, *AJ*, 145, 46
- Lim, B., Sung, H., Bessell, M. S., Kim, J. S., Hur, H., & Park, B.-G. 2015, Sejong open cluster survey (SOS) - IV. The young open clusters NGC 1624 and NGC 1931, *AJ*, 149, 127
- Lim, B., Sung, H., Karimov, R., & Ibrahimov, M. 2011, Sejong open cluster survey. I. NGC 2353, *J. Korean Astron. Soc.*, 44, 39
- Lim, B., Sung, H., Kim, J. S., Bessell, M. S., & Karimov, R., 2014a, Sejong open cluster survey (SOS) - II. IC 1848 cluster in the H II region W5 west, *MNRAS*, 438, 1451
- Lim, B., Sung, H., Kim, J. S., Bessell, M. S., & Park, B.-G. 2014b, Sejong open cluster survey (SOS) - III. The young open cluster NGC 1893 in the H II region W8, *MNRAS*, 443, 454
- Lo, K. Y., & Burke, B. F. 1973, H<sub>2</sub>O sources in Sharpless H II regions, *A&A*, 26, 487
- Menzies, J. W., Marang, F., Laing, J. D., Coulson, I. M., Engelbrecht, C. A. 1991, *UBV(RI)c* photometry of equatorial standard stars - A direct comparison between the northern and southern systems, *MNRAS*, 248, 642
- Minier, V., Burton, M. G., Hill, T., Pestalozzi, M. R., Purcell, C. R., Garay, G., Walsh, A. J., & Longmore, S. 2005, Star-forming protoclusters associated with methanol masers, *A&A*, 429, 945
- Minier, V., Peretto, N., Longmore, S. N., Burton, M. G., Cesaroni, R., Goddi, C., Pestalozzi, M. R., & André, Ph. 2007, Anatomy of the S255S257 complex triggered high-mass star formation, in *Proc. IAU Symp. 237, Triggered Star Formation in a Turbulent ISM*, ed. B. Elmegreen & J. Palous (Cambridge: Cambridge Univ. Press), 160
- Moffat, A. F. J., Jackson, P. D., & Fitzgerald, M. P. 1979, The rotation and structure of the galaxy beyond the solar circle. I - Photometry and spectroscopy of 276 stars in 45 H II regions and other young stellar groups toward the galactic anticentre, *A&AS*, 38, 197
- Morris, M., Palmer, P., Turner, B. E., & Zuckerman, B. 1974, Millimeter-wavelength molecular lines and far-infrared sources, *ApJ*, 191, 349
- Mucciarelli, P., Preibisch, T., & Zinnecker, H. 2011, Revealing the "missing" low-mass stars in the S254-S258 star forming region by deep X-ray imaging, *A&A*, 533, 121
- Park, B.-G., & Sung, H. 2002, *UBVI* and *H $\alpha$*  photometry of the young open cluster NGC 2244, *AJ*, 123, 892
- Park, B.-G., Sung, H., Bessell, M. S., & Kang, Y. H. 2000, The pre-main-sequence stars and initial mass function of NGC 2264, *AJ*, 120, 894
- Pismis, P., & Hasse, I. 1976, Study of a triple emission nebula in Orion, *Ap&SS*, 45, 79
- Porras, A., Christopher, M., Allen, L., et al. 2003, A catalog of young stellar groups and clusters within 1 kiloparsec of the sun, *AJ*, 126, 1916
- Robitaille, T. P., Whitney, B. A., Indebetouw, R., & Wood, K. 2007, Interpreting spectral energy distributions from young stellar objects. II. Fitting observed SEDs using a large grid of precomputed models, *ApJS*, 169, 328
- Russeil, D., Adami, C., & Georgelin, Y. M. 2007, Revised distances of Northern HII regions, *A&A*, 470, 161
- Salpeter E. E., 1955, *ApJ*, The luminosity function and stellar evolution, 121, 161
- Sharpless, S. 1959, A catalogue of H II regions, *ApJS*, 4, 257
- Siess, L., Dufour, E., & Forestini, M. 2000, An internet server for pre-main sequence tracks of low- and intermediate-mass stars, *A&A*, 358, 593
- Skrutskie, M. F., et al. 2006, The two micron all sky survey (2MASS), *AJ*, 131, 1163
- Sota, A., Maíz A. J., Walborn, N. R., Alfaro, E. J., Barbá, R. H., Morrell, N. I., Gamen, R. C., & Arias, J. I. 2011, The Galactic O-star spectroscopic survey. I. Classification system and bright northern stars in the blue-violet at  $R \sim 2500$ , *ApJS*, 193, 24
- Sung, H., & Bessell, M. S. 2004, The initial mass function and stellar content of NGC 3603, *AJ*, 127, 1014
- Sung, H., & Bessell, M. S. 2010, The initial mass function and young brown dwarf candidates in NGC 2264 IV. The initial mass function and star formation history, *AJ*, 140, 2070
- Sung, H., & Bessell, M. S. 2014, The interstellar reddening law within 3kpc from the sun, in *ASP Conf. Ser. 482, the 10th Pacific Rim Conference on Stellar Astrophysics*, ed. H.-W. Lee, Young Woon Kang, and Kam-Ching Leung (San Francisco, CA: ASP), 275
- Sung, H., Bessell, M. S., & Chun, M.-Y. 2004, The initial mass function and young brown dwarf candidates in NGC 2264. I. The initial mass function around S Monocerotis, *AJ*, 128, 1684
- Sung, H., Bessell, M. S., Chun, M.-Y., Karimov, R., & Ibrahimov, M. 2008, The initial mass function and young

- brown dwarf candidates in NGC 2264 III. Photometric data, *AJ*, 135, 441
- Sung H., Bessell M. S., & Lee S.-W. 1997, *UBVRI*  $H\alpha$  photometry of the young open cluster NGC 2264, *AJ*, 114, 2644
- Sung, H., Bessell, M. S., & Lee, S.-W. 1998, *UBVRI* and  $H\alpha$  photometry of the young open cluster NGC 6231, *AJ*, 115, 734
- Sung, H., Chun, M.-Y., & Bessell, M. S. 2000, *UBVRI* and  $H\alpha$  photometry of the young open cluster NGC 6530, *AJ*, 120, 333
- Sung, H., Lim, B., Bessell, M. S., Kim, J. S., Hur, H., Chun, M.-Y., & Park, B.-G. 2013a, Sejong open cluster survey (SOS). 0. Target selection and data analysis, *J. Korean Astron. Soc.*, 46, 103 (Paper 0)
- Sung, H., Sana, H., & Bessell, M. S. 2013b, The initial mass function and the surface density profile of NGC 6231, *AJ*, 145, 37
- Sung, H., Stauffer, J. R., Bessell, M. S. 2009, A *Spitzer* view of the young open cluster NGC 2264, *AJ*, 138, 1116
- Turner, B. E. 1971, Anomalous OH emission from new types of Galactic objects, *Astrophys. Lett.*, 8, 73
- Walborn N. R. 1971, Some spectroscopic characteristics of OB stars: an investigation of the space distribution of certain OB stars and the reference frame of the classification, *ApJS*, 23, 257
- Walborn, N. R., & Fitzpatrick, E. L. 1990, Contemporary optical spectral classification of the OB stars - A digital atlas, *PASP*, 102, 379
- Wang, Y., Beuther, H., Bik, A., Vasyunina, T., Jiang, Z., Puga, E., Linz, H., Rodón, J. A., Henning, Th., & Tamura, M. 2011, Different evolutionary stages in the massive star-forming region S255 complex, *A&A*, 527, 32
- Whittet, D. C. B. 1977, The dependence of the extinction ratio on galactic longitude, *MNRAS*, 180, 29
- Zinchenko, I., Liu, S.-Y., Su, Y.-N., Kurtz, S., Ojha, D. K., Samal, M. R., & Ghosh, S. K. 2012, A multi-wavelength high-resolution study of the S255 star-forming region: General structure and kinematics, 755, 177